Article

Neuron

Optogenetic Activation of Normalization in Alert Macaque Visual Cortex

Highlights

- Optogenetic depolarization of excitatory neurons activates normalization in V1
- Activated circuits mediate competition between optogenetic and visual stimulation
- This competition can be biased by elevating the intensity of each stimulus
- The normalization model provides excellent fits to these stimulus interactions

Authors

Jonathan J. Nassi, Michael C. Avery, Ali H. Cetin, Anna W. Roe, John H. Reynolds

Correspondence

nassi@snl.salk.edu

In Brief

The Normalization Model can account for a wide variety of neural computations, ranging from contrast gain control to attentional selection. Here, Nassi et al. find strong support for the model by combining optogenetic and visual stimulation in primate visual cortex.

Nassi et al., 2015, Neuron *86*, 1504–1517
June 17, 2015
http://dx.doi.org/10.1016/j.neuron.2015.05.040

CellPress

CellPress

Neuron
Article

Optogenetic Activation of Normalization in Alert Macaque Visual Cortex

Jonathan J. Nassi,[1,*] Michael C. Avery,[1] Ali H. Cetin,[1,4] Anna W. Roe,[2,3] and John H. Reynolds[1]
[1]Systems Neurobiology Laboratories, Salk Institute for Biological Studies, La Jolla, CA 92037, USA
[2]Department of Psychology, Vanderbilt University, Nashville, TN 37203, USA
[3]Zhejiang University Interdisciplinary Institute of Neuroscience and Technology (ZIINT), Zhejiang University, 310027 Hangzhou, China
[4]Present address: Allen Institute for Brain Science, Seattle, WA, 98103, USA
*Correspondence: nassi@snl.salk.edu
http://dx.doi.org/10.1016/j.neuron.2015.05.040

SUMMARY

Normalization has been proposed as a canonical computation that accounts for a variety of nonlinear neuronal response properties associated with sensory processing and higher cognitive functions. A key premise of normalization is that the excitability of a neuron is inversely proportional to the overall activity level of the network. We tested this by optogenetically activating excitatory neurons in alert macaque primary visual cortex and measuring changes in neuronal activity as a function of stimulation intensity, with or without variable-contrast visual stimulation. Optogenetic depolarization of excitatory neurons either facilitated or suppressed baseline activity, consistent with indirect recruitment of inhibitory networks. As predicted by the normalization model, neurons exhibited sub-additive responses to optogenetic and visual stimulation, which depended lawfully on stimulation intensity and luminance contrast. We conclude that the normalization computation persists even under the artificial conditions of optogenetic stimulation, underscoring the canonical nature of this form of neural computation.

INTRODUCTION

The brain is a highly modular structure with different areas specialized to efficiently process disparate types of sensory information and to inform a large repertoire of behavioral goals (Zeki and Shipp, 1988). It is widely believed that canonical circuits and computations exist within this modular design such that, for instance, the same basic computation can be utilized in different contexts and across different brain regions (Douglas and Martin, 2004). One such example is divisive normalization, whereby a ratio is computed between the driving input to an individual neuron and the overall activity level of the network in which the neuron is embedded. This relatively simple computation has several attractive features related to coding efficiency and has been proposed to operate across a wide range of brain areas, modalities, and species (Carandini and Heeger, 2012). The normalization model has been used to account for several ways in which neuronal responses change across sensory conditions and has recently been extended to account for neuronal response modulation associated with different cognitive states, such as during directed attention and decision making (Reynolds and Heeger, 2009; Lee and Maunsell, 2009; Louie et al., 2013).

Normalization has been successful in accounting for a variety of non-linear response properties that are observed in multiple areas including retina and visual cortex (Sperling and Sondhi, 1968; Grossberg, 1973; Albrecht and Geisler, 1991; Heeger, 1992; Carandini et al., 1997; Zoccolan et al., 2005). Originally developed to account for response saturation and contrast-invariant tuning in primary visual cortex (V1), normalization has since been applied to more complex stimulus configurations such as cross-orientation suppression and surround suppression (Heeger, 1992; Carandini et al., 1997; Cavanaugh et al., 2002). In the case of cross-orientation suppression, a non-preferred stimulus that evokes a weak response on its own can be strongly suppressive when superimposed over a preferred stimulus (Morrone et al., 1982). This form of non-specific suppression can be explained by postulating the existence of a broadly tuned "normalization pool" that provides a divisive signal that scales neuronal activity by the reciprocal of its summed activity. Accordingly, the response of a neuron to any particular stimulus configuration will depend on the strength of its excitatory drive relative to the summed activity of this normalization pool.

We are early in our understanding of the neural mechanisms underlying this fundamental computation. Recent studies have implicated several different visual cortical circuit elements in normalization, including feedback connections, lateral excitatory connections, and local inhibitory interneurons (Adesnik and Scanziani, 2010; Adesnik et al., 2012; Nassi et al., 2013, 2014; Sato et al., 2014). For instance, Sato et al. (2014) showed that optogenetic activation of laterally projecting neurons in anesthetized mouse V1 modulated visual responses in a contrast-dependent manner consistent with normalization. Natural visual stimulation probably engages such highly specific circuitry, but the normalization model stipulates that whatever neural circuitry is involved, the neuronal response is ultimately governed by the ratio of driving inputs to suppressive inputs, regardless of the particular route by which those inputs are activated. Therefore, a prediction of the model is that normalization computations

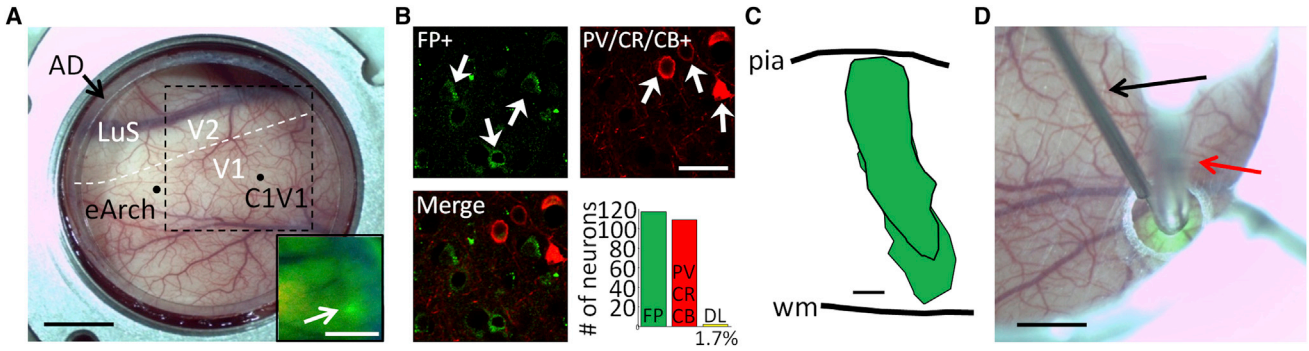

Figure 1. Excitatory Neurons in Primary Visual Cortex Targeted for Optogenetic Stimulation

(A) Transparent artificial dura (AD) cranial window implanted over the left occipital cortex in monkey A. Lentivirus (lenti-CaMKIIα-C1V1$_{E162T}$-ts-EYFP) encoding the depolarizing opsin C1V1 was injected at a single location within primary visual cortex (V1), posterior to the lunate sulcus (LuS) and the border (dashed white line) between V1 and the secondary visual area (V2). Adeno-associated virus (AAV5-CaMKIIα-eArch3.0-ts-EYFP) encoding the hyperpolarizing opsin eArch3.0 was injected 5 months later at a second, distant location within V1. Dashed black square indicates borders of image shown in inset. Scale bar, 5 mm. Inset: approximately 3 weeks after lentivirus injection, enhanced yellow fluorescent protein (EYFP) expression was detected at the expected cortical location (white arrow). Scale bar, 5 mm.

(B) Histological analysis in a separate monkey confirmed that expression of C1V1 and EYFP was biased almost exclusively to excitatory neurons at and around the injection site. White arrows indicate neurons immuno-positive for EYFP (FP+; green, top-left panel) or the inhibitory neuron markers parvalbumin, calretinin, or calbindin (PV/CR/CB+; red, top-right panel) but not both (Merge; yellow, bottom-left panel). Only 1.7% of all EYFP-positive neurons counted (n = 119 across five different fields of view) were double labeled for both EYFP and PV/CR/CB (n = 2) (bottom-right panel), indicating that expression was heavily biased toward excitatory neurons. Scale bar, 20 μm.

(C) Histological analysis confirmed that the lentivirus used in these studies expresses across the entire cortical depth, including superficial layers. Green regions denote expression of EYFP across two analyzed sections separated by 100 μm. Expression of EYFP was observed from just below the pia to just above the white matter (wm). Scale bar, 250 μm.

(D) Simultaneous extracellular recordings and optogenetic stimulation was carried out by penetrating the AD at an angle with a thin glass-coated tungsten electrode (black arrow) and placing a 600-μm-diameter multi-mode fiber just above the AD and over the recording site (red arrow). 532 nm laser light was collimated into the fiber and directed through the AD toward the cortical surface. The cortical location shown in (D) was examined as part of separate control experiments and, therefore, was not aligned with the injection site indicated in (A). Scale bar, 2 mm.

should occur even if driven by highly arbitrary patterns of activation that are not normally induced by natural sensory input. To test this, we used an artificial form of stimulation: optogenetic activation of excitatory neurons in V1 expressing a depolarizing opsin. This form of stimulation differs from natural visual stimulation in that it is initiated by the excitatory neurons that happen to express opsin and that are located within the superficial layers of cortical tissue, where laser illumination is strong enough to activate them. We measured changes in neuronal activity in alert macaque V1 as a function of laser intensity and tested whether optogenetic activation would modulate visually evoked responses in a manner predicted by the normalization model. The normalization model made multiple, testable predictions about the nature of optogenetic modulation, each of which was confirmed experimentally. These experiments show that normalization is robust to the nature of driving inputs and open the door to the use of optogenetic stimulation as a means to study this canonical form of neural computation.

RESULTS

We set out to test the normalization model by directly activating excitatory neurons in alert macaque V1. To do so, we implanted an artificial dura optical window (Ruiz et al., 2013) over V1 in each of two macaques (monkeys A and M) and injected a lentivirus encoding the depolarizing opsin C1V1 (Yizhar et al., 2011b) throughout the entire depth of cortex at a single location (Figure 1A). We used a lentivirus with the alpha calcium/calmodulin-dependent protein kinase II (CaMKIIα) promoter to preferentially drive expression of C1V1 and enhanced yellow fluorescent protein (EYFP) among excitatory neurons at the injection site (Han et al., 2009). In vivo epi-fluorescence imaging confirmed viral expression at the targeted site several weeks after injection (Figure 1A, inset). We assessed specificity of viral expression to excitatory neurons in a separate monkey, finding essentially no overlap between neurons expressing EYFP and inhibitory neurons expressing parvalbumin, calretinin, or calbindin—which together account for over 95% of all inhibitory neurons in macaque V1 (Van Brederode et al., 1990; Meskenaite 1997) (Figure 1B). We also confirmed in this same monkey that viral expression was present across the entire cortical depth, with no bias toward any particular layer (Figure 1C).

Responses to Optogenetic Stimulation Alone

Excitatory neurons local to the injection site were depolarized by delivering 532 nm laser light through an optical fiber positioned directly above the artificial dura window overlying the cortex (Figure 1D). We estimated the spot size of illumination at the cortical surface to have a diameter of approximately 1.9 mm, such that the entire patch of cortex expressing EYFP (approximately 680 μm diameter) was stimulated (see Supplemental Experimental Procedures). We recorded from 249 units within this stimulated patch of cortex (142 monkey A, 107 monkey M) and

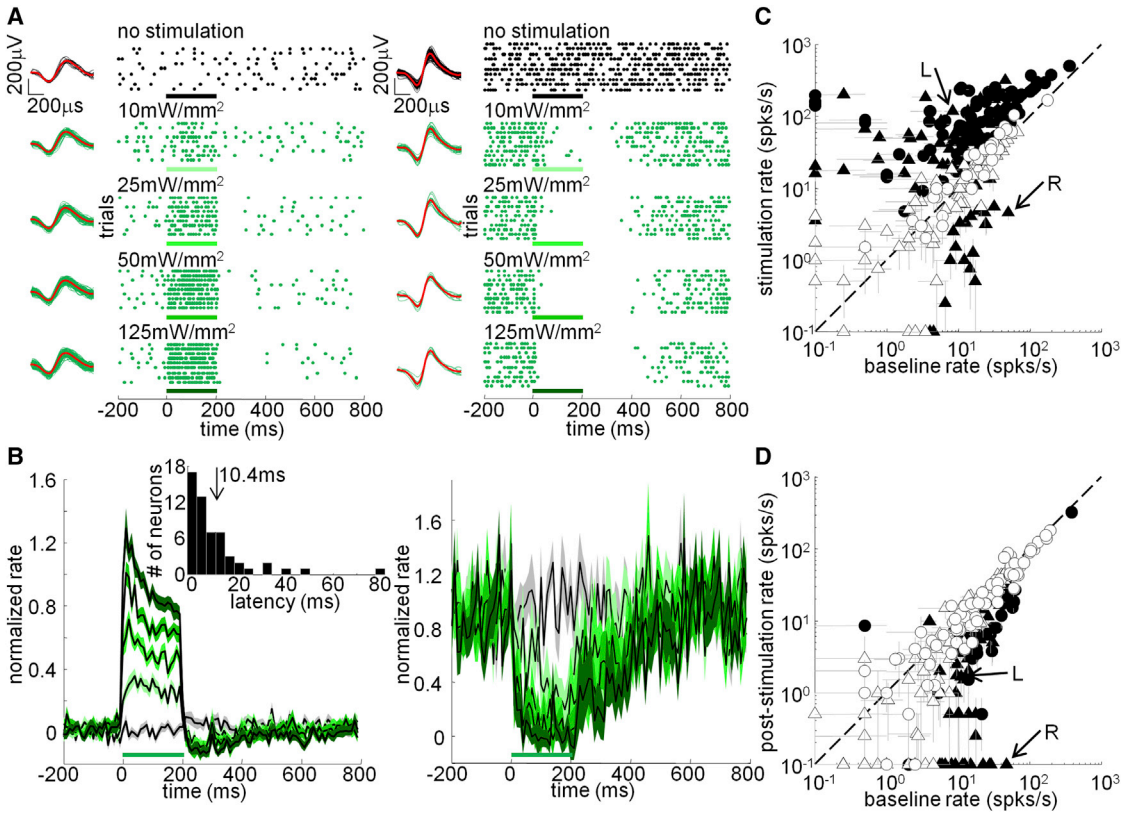

Figure 2. Optogenetic Depolarization of Excitatory Neurons in V1 Generates Both Excitation and Inhibition

(A) Rasters indicating the time of action potentials on trials with (green dots) or without (black) 200 ms continuous optogenetic stimulation for two example single units. Each row is a separate trial. Four different stimulation intensities (10, 25, 50, and 125 mW/mm^2) were tested. The action potential waveforms associated with each stimulation condition are presented to the left of the rasters (average waveforms for each condition are in red).

(B) Normalized average post-stimulus time histograms (PSTHs; black) for all significantly facilitated (left; n = 137) and suppressed (right; n = 23) neurons (single and multi-units combined). SE presented with gray indicating no stimulation condition and different shades of green from light to dark indicating stimulation of increasing intensity. Inset: response-onset latency distribution for significantly facilitated single units (n = 55; mean = 10.4 ± 1.9 SE).

(C) Mean ± SE rates with and without optogenetic stimulation (125 mW/mm^2) for the entire population (n = 249). Rates were calculated within a 200 ms time window aligned with stimulus onset. 126 units were significantly facilitated (47 single units, 79 multi-units) and 21 were suppressed (21 single units, 0 multi-units) at the highest intensity tested. Arrows indicate single-unit examples from (A) (L indicates the unit to the left, R to the right). Triangles indicate single units, circles indicate multi-units, and filled symbols indicate significant optogenetic modulation (Wilcoxon rank-sum test, $p < 0.05$).

(D) Same as in (C) but for a post-stimulation time window 10–210 ms following stimulation offset. Two units were significantly facilitated (1 single unit, 1 multi-unit) and 66 were suppressed (44 single units, 24 multi-units) following optogenetic stimulation at the highest intensity tested. See also Figures S1 and S2.

measured responses to optogenetic stimulation (200 ms, continuous) of varying intensity (0, 10, 25, 50, and 125 mW/mm^2 measured at the fiber tip) while the monkeys fixated the center of a monitor with a neutral-gray luminance background. We found that 160 units (77 single neurons, 83 multi-units) were significantly modulated, relative to baseline, in response to at least one stimulation intensity tested (Wilcoxon rank-sum test, $p < 0.05$, Bonferroni corrected for multiple comparisons) (Figure 2). Control studies confirmed that these effects were wavelength dependent and, therefore, specific to optogenetic activation rather than a heat or electro-optical artifact (Figure S1). The most common effect was a significant increase in firing rate in response to light (137 units; 55 single, 82 multi), as expected following the activation of the depolarizing opsin C1V1 (Figures 2A–2C). For some of these neurons (17 of 55 facilitated single units), response latency was short ($\leq$2 ms at the highest intensity tested), consistent with direct depolarization of neurons expressing opsin. However, response latency varied considerably across the population of facilitated single units (mean = 10.4 ms ± 1.9 SE) (Figure 2B, inset). This could be an indirect consequence of variation in opsin expression and light scatter across cortical depths, which would, in turn, lead to variation in effective stimulation intensity and response latency for directly depolarized neurons. An alternative possibility is that longer latencies result from variation in the number of synapses and, therefore, synaptic delays between indirectly depolarized neurons and their directly depolarized input.

While the most common effect of optogenetic stimulation was facilitation, we also observed many cases of significant suppression of spontaneous activity (23 units; 22 single, 1 multi) (Figures 2A–2C). Given that the opsin is depolarizing and was expressed selectively in excitatory neurons, this reduction in firing rate was

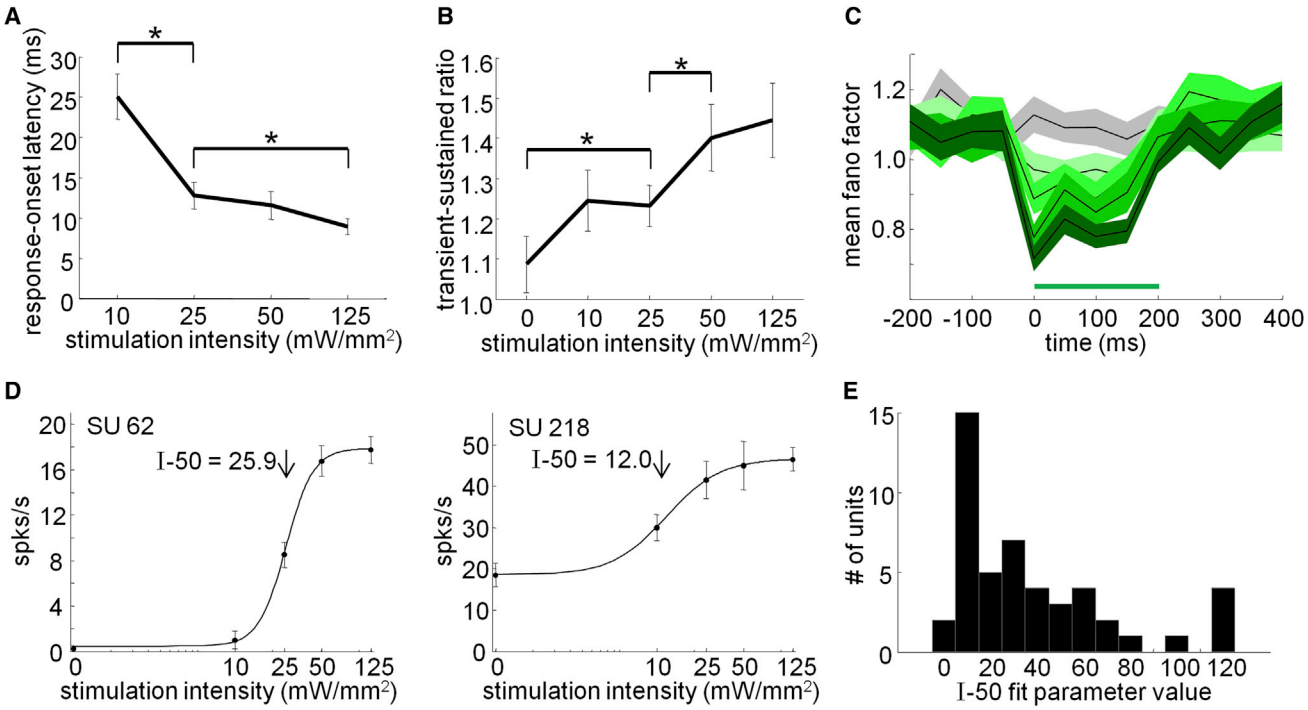

Figure 3. Intensity-Dependent Neural Response Properties of Optogenetic Stimulation

(A) Optogenetic response-onset latency (ms) as a function of stimulation intensity (mW/mm^2) for all significantly facilitated units in the population (n = 137). Mean ± SE presented. Asterisks indicate significant differences in latency across conditions (paired t test, $p < 0.05$).

(B) Optogenetic transient-to-sustained response ratio as a function of stimulation intensity (mW/mm^2) for all significantly facilitated units in the population (n = 137). Mean ± SE presented. Asterisks indicate significant differences in ratio across conditions (Wilcoxon signed-rank test, $p < 0.05$).

(C). Mean Fano factor time courses (black) for all significantly facilitated units (n = 137). SE presented with gray indicating no stimulation condition and different shades of green from light to dark indicating stimulation of increasing intensity. See also Figure S3.

(D) Single-unit example intensity response functions from monkey A (single unit #62; left) and monkey M (single unit #218, right). Mean ± SE presented. Curves produced from hyperbolic ratio function fits. The intensity that produced half-maximal response (I-50) indicated with arrow.

(E) Distribution of I-50 fit parameter values across all significantly facilitated units in the population. Only units that were well fit by the hyperbolic ratio function were included (explained variance (R^2) $\geq$ 0.7; n = 48).

probably mediated through indirect activation of inhibitory neurons (Mateo et al., 2011). The total number of suppressed units in the recorded population was probably underestimated due to a floor effect caused by low spontaneous firing rates. An indication of widespread inhibition during optogenetic stimulation was post-stimulation suppression (10–210 ms following stimulation offset) that we often observed in significantly modulated neurons (62/160 units; 40 single, 22 multi; Wilcoxon rank-sum test, $p < 0.05$, Bonferroni corrected for multiple comparisons) (Figure 2D). This post-stimulus suppressive effect was not simply due to spike-rate adaptation or synaptic depletion following optogenetic facilitation—as 65% of units that were suppressed during stimulation exhibited significantly reduced ongoing activity during the post-stimulation period. Furthermore, it did not require long periods of time to build up, as we observed similar suppression following short duration (5 ms) pulsed stimulation as well (Figure S2). The observed suppression both during and immediately following stimulation thus provides evidence that the initial depolarization of excitatory neurons generated excitation as well as strong and consistent inhibition.

Optogenetic stimulation produced neuronal responses that changed with elevation of stimulation intensity in ways that parallel non-linear changes in visually evoked responses that occur with elevation of luminance contrast. These parallels were likely due to a combination of indirect network effects and intrinsic properties of the C1V1 opsin itself (Mattis et al., 2012). Among these were reductions in response latency with increases in stimulation intensity (Figures 2B and 3A) and elevations in the transient-to-sustained response ratio with increases in stimulation intensity (Figures 2B and 3B). We also observed an intensity-dependent reduction in neural variability (Fano factor) that coincided with the onset of optogenetic stimulation (Figure 3C), similar to the decline in variability at stimulus onset that has been reported previously across several different cortical areas and experimental contexts (Churchland et al., 2010). This reduction in Fano factor remained significant for mean-matched firing rate distributions and, therefore, was not simply an artifact of firing rate increase (Figure S3). Perhaps the most striking parallel was the sigmoidal intensity response functions often observed with variation in stimulation intensity (Figure 3D). The observed response saturation for high-intensity stimulation is reminiscent of response saturation with elevation of luminance contrast. Accordingly, across all facilitated units (n = 137), the mean firing rates were well fit by a hyperbolic ratio function typically used to

describe visual contrast response functions (mean explained variance = 93% ± 1.7% SE). The stimulation intensity that produced half-maximal response (I-50) was obtained from each fit and was found to vary substantially across the population (Figure 3E). Other parameters of the fit, including slope, varied substantially as well, indicating a wide range of sensitivities to optogenetic stimulation. Despite the artificial pattern of activation produced by optogenetic stimulation, the resultant intensity-dependent neuronal response profiles were remarkably similar to those typically observed following visual stimulation of varying luminance contrast.

Optogenetic Modulation of Visually Evoked Responses

We next investigated how the mix of direct and indirect network activation generated by optogenetic stimulation modulates the neural response evoked by a visual stimulus. This approach is akin to previous studies that have examined the interactions between pairs of visual stimuli. These studies have found that the response evoked by one visual stimulus can often be suppressed by the addition of a second stimulus, even if the second stimulus evokes an excitatory response when presented alone (Morrone et al., 1982; Snowden et al., 1991; Carandini et al., 1997; Reynolds et al., 1999; Reynolds and Desimone, 2003). Here, however, we have replaced one of the two visual stimuli with optogenetic stimulation that bypasses the natural feedforward pattern of activation along the retino-geniculo-cortical pathway and, instead, introduces artificial excitatory drive directly into the local cortical circuit in V1. We presented drifting sinusoidal gratings centered within the receptive field and matched to each recorded unit's preferred size (median diameter = 0.63°), orientation, and spatial and temporal frequencies. We estimated that the optogenetically stimulated patch of cortex corresponded to an aggregate visual field diameter of approximately 0.86° at the eccentricities studied (see Supplemental Experimental Procedures) (Van Essen et al., 1984). The contrast of the visual stimulus (0%, 6%, 12%, 25%, 50%, and 99%) and the intensity of optogenetic stimulation (median values: 0, 10, 30, and 80 mW/mm^2) varied randomly across trials. The onset of optogenetic stimulation was simultaneous with visual stimulus onset and both types of stimuli lasted at least 200 ms in duration. We chose a time window for analysis over which responses to both visual and optogenetic stimulation had typically settled to a stable sustained rate, a 100 ms window beginning 100 ms after visual and optogenetic stimulation onset. We measured visual-optogenetic interactions for 116 units (40 monkey A, 76 monkey M), 93 of which were sensitive to both visual contrast and stimulation intensity and were therefore analyzed further (two-way ANOVA, $p < 0.05$). Seventy-six of these 93 units (34 single, 42 multi) were significantly modulated, relative to baseline, in response to the highest stimulation intensity tested (Wilcoxon rank-sum test, $p < 0.05$). Sixty-four were facilitated and 12 were suppressed. In 42 of 64 cases (66%), if optogenetic stimulation facilitated the baseline response, it also led to significant facilitation of the visually evoked response for at least one luminance contrast (Wilcoxon rank-sum test, $p < 0.05$, Bonferroni corrected for multiple comparisons across visual contrasts) (Figure 4A). For a significant minority of cases (11/64 units, 17%), optogenetic stimulation that evoked an excitatory response when presented alone caused significant suppression of the visually evoked response (Figure 4B). When stimulation suppressed the baseline response, the visual response was almost always suppressed and never facilitated (10 of 12 units, 83%, significantly suppressed) (Figure 4C). For the 17 units with no stimulation effect at baseline, 9 were suppressed during the visual response and none were facilitated. Control experiments indicated that these effects were relatively fast and stable in sign (Figure S4). In total, the visual responses of 42 units were facilitated and 30 units were suppressed by optogenetic stimulation.

Modeling Optogenetic Modulation

If, as we hypothesize, optogenetic stimulation of excitatory drive activates normalization circuitry, then visual and optogenetic stimulation should interact as predicted by the normalization model (Carandini and Heeger, 2012). To test this, we extended the normalization model as in Sato et al. (2014) to incorporate a laser-evoked excitatory drive that, in turn, indirectly activated divisive suppression and applied it to our data. The model was governed by the following normalization equation:

$$R(c,\lambda) = [R_m * (R_o + c^n + \lambda^m D)/(\sigma + c^n + \lambda^m S)] + , \quad \text{(Equation 1)}$$

where c and λ indicate visual contrast and optogenetic stimulation intensity, R_o is proportional to the baseline firing rate, R_m scales the maximum firing rate, n and m independently control the neuron's sensitivity to elevations of visual contrast and optogenetic stimulation intensity, σ is the semi-saturation constant, and D and S are the excitatory drive and divisive suppression evoked by optogenetic stimulation. The response was then half-rectified.

The model makes several predictions as to how visual and optogenetic stimulation will interact. One prediction is that visual and optogenetic stimulation will typically combine sub-additively. That is, the response to simultaneous visual and optogenetic stimulation will typically be less than the sum of the responses evoked by the visual and optogenetic stimulus, when they are presented separately. This is a robust property of the model, as illustrated in Figure 4D, where we simulated 55 neurons with randomly assigned model parameter values (see Experimental Procedures). The combined responses of these simulated neurons were almost always smaller than the sum of the individual responses. This sub-additive interaction held for a relatively large range of simulated D and S values, indicating that the predicted behavior does not depend on the particular strength of excitatory drive and divisive suppression evoked by optogenetic stimulation.

Measured responses to simultaneous visual and optogenetic stimulation also displayed this property. Close inspection of example single units of facilitation and suppression show that the pair response was not a simple sum of the two individual responses (Figures 4A–4C). This was true for the entire population and across all contrasts and stimulation intensities tested (Figure 4E). We quantified this according to an index [pair response / (laser-only response + visual-only response)] that equaled one for an additive pair response and below or above one for a sub-additive or supra-additive pair response, respectively. The median of this index (0.67 ± 0.02 SE) indicated that the combined responses were almost always sub-additive,

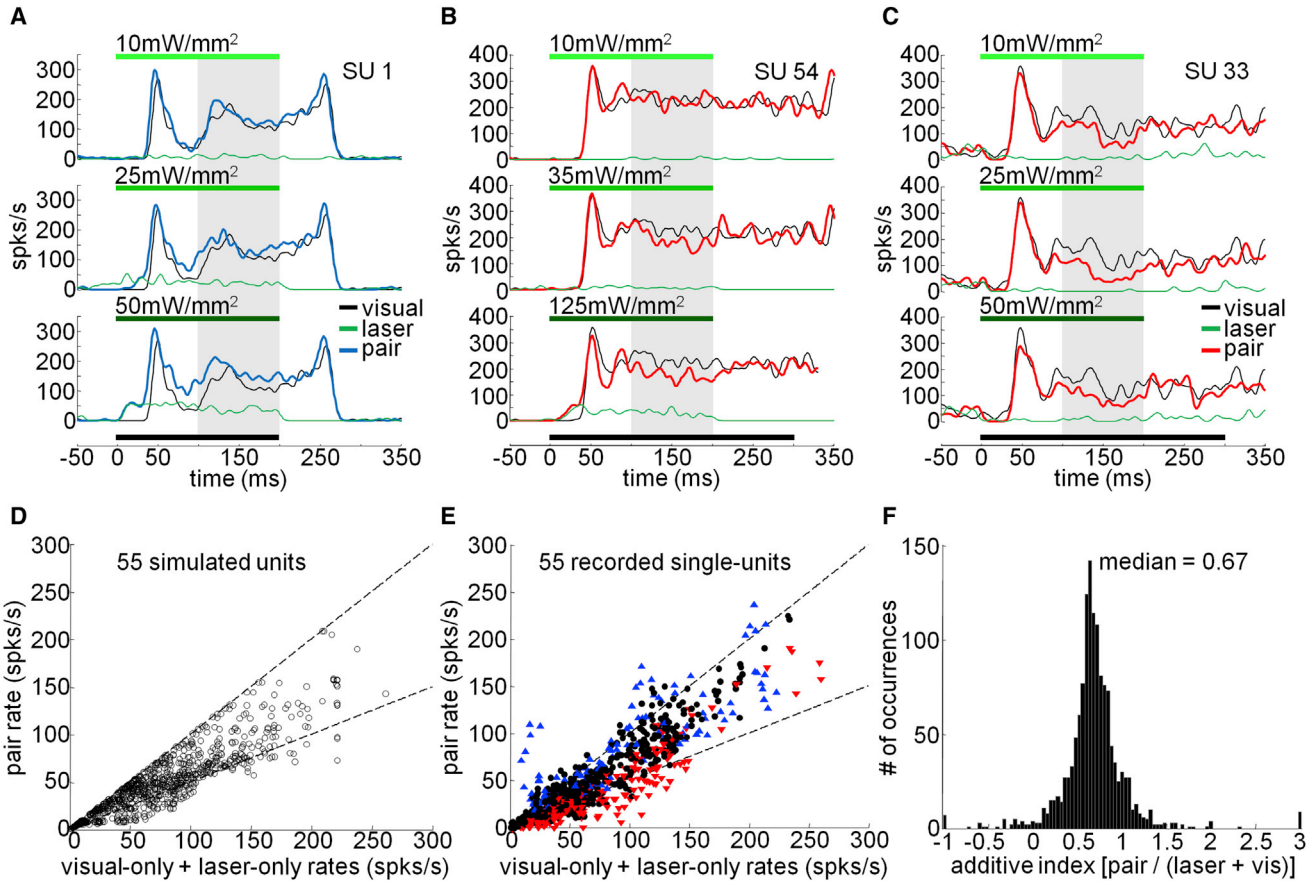

Figure 4. Simultaneous Visual and Optogenetic Stimulation Produces Sub-additive Responses as Predicted by Normalization Model

(A–C) Single-unit example PSTHs during presentation of a 99% contrast visual stimulus and optogenetic stimulation of varying intensities (increasing intensity from top to bottom). Mean rates for visual-only (black), laser-only (green), and pair (blue for facilitation, red for suppression) are presented. Black bars indicate timing of visual stimulus presentation and green bars indicate timing of optogenetic stimulation. Gray-shaded region denotes the 100–200 ms time window following onset of visual and optogenetic stimulation from which spike rates were calculated in (E) and (F).

(D and E) Mean rates (baseline-subtracted) during simultaneous visual and optogenetic stimulation (pair rate) as a function of the summed visual-only and laser-only responses for 55 model-simulated units (D) and 55 recorded single units (E). Pair rates for five different visual contrast conditions (6%, 12%, 25%, 50%, and 99%) and three different optogenetic stimulation intensity conditions (low, mid, and high) are presented. Each unit accounts for 15 data points. Dashed lines indicate the predicted pair response according to a sum or average of the visual-only and laser-only responses. Blue upward and red downward triangles indicate significant optogenetic facilitation and suppression, respectively (Wilcoxon rank-sum test, $p < 0.05$).

(F) Distribution of additive index [pair response / (visual-only + laser-only)] across the entire population (median = 0.67 ± 0.02; n = 93). An index of one indicates a perfectly additive pair response, whereas indices less than or greater than one indicate sub-additive or supra-additive pair responses respectively. See also Figure S4.

typically falling somewhere between the average and the sum of the individual responses (Figure 4F).

A second prediction of the model is that the combined responses will depend systematically on the visual contrast and optogenetic stimulation intensity, with each stimulus exerting influence over firing rate according to a weighted sum of the individual stimulus-evoked responses. This is also readily apparent from model simulations appearing in Figure 5C. To illustrate this model prediction, we fit the model responses with the following weighted sum equation:

$$Rp(c,\lambda) = w_V(c,\lambda)Rv(c) + w_L(c,\lambda)Rs(\lambda), \qquad \text{(Equation 2)}$$

where the pair response $Rp(c,\lambda)$ to a visual stimulus with contrast c and optogenetic stimulation with intensity λ is given by the linear combination of the responses to visual $Rv(c)$ and optogenetic stimulation $Rs(\lambda)$ alone. The scaling factors w_V, w_L were allowed to vary depending on the combination of visual contrast and stimulation intensity, to obtain a pair of weights for each combination that provided the best fit to the model responses across all 10,000 simulated neurons (Figure 5C). Best-fitting weights were consistently below unity and depended markedly on contrast and stimulation intensity, ranging from near-equal weights to winner-take-all. This type of behavior is one of the hallmarks of cross-orientation suppression caused by overlapping visual stimuli in V1 (Busse et al., 2009). This prediction of the model also held for a relatively large range of simulated D and S values.

To test this prediction, we fit the data with the same weighted sum equation. The best-fitting weights for observed responses

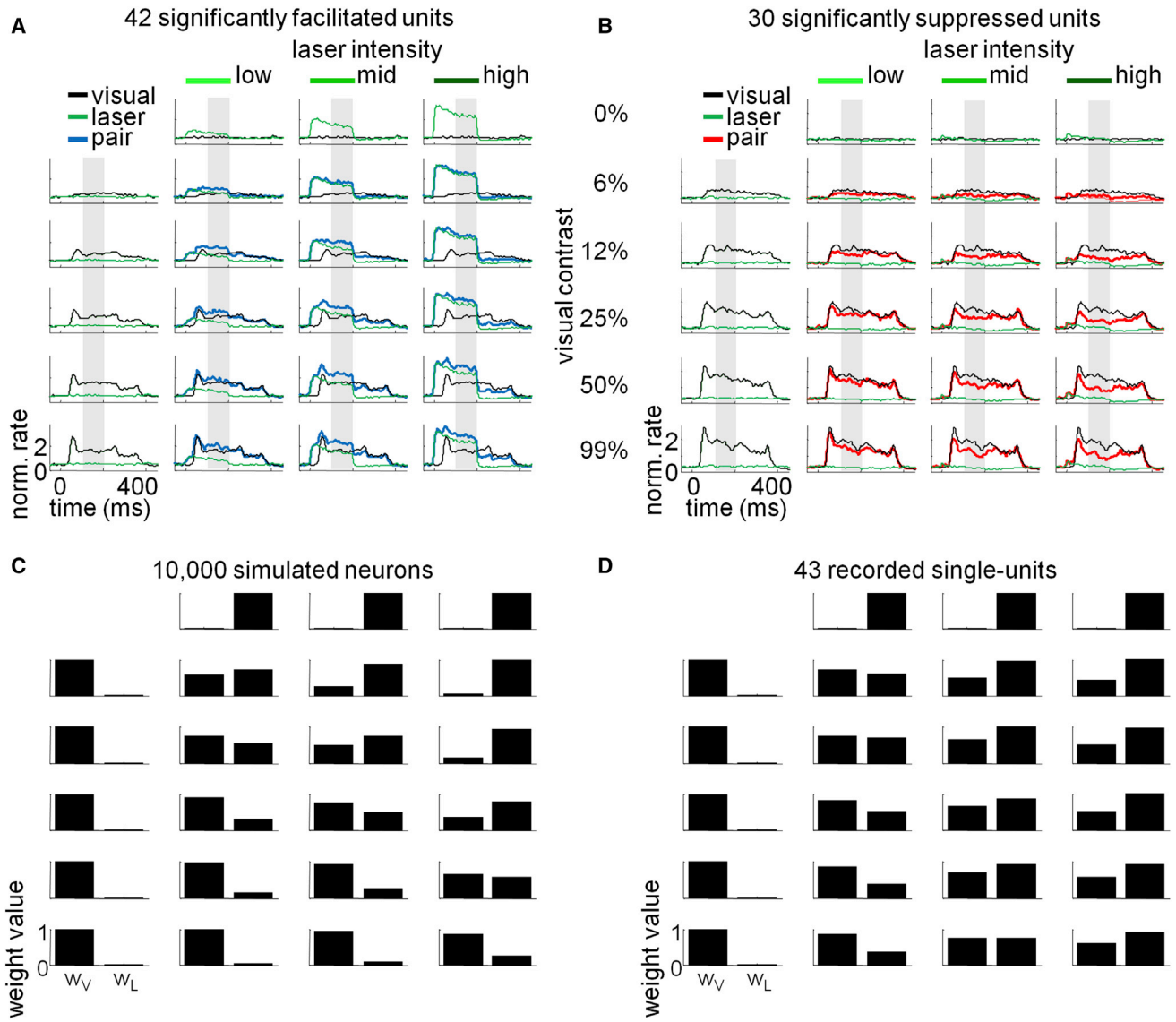

Figure 5. Competitive Interactions between Visual and Optogenetic Stimulation as Predicted by Normalization Model

(A and B) Normalized average PSTHs for units with visual responses significantly facilitated (left) or suppressed (right) by optogenetic stimulation (Wilcoxon rank-sum test, $p < 0.05$). Each row indicates a different visual contrast condition and each column a different optogenetic stimulation intensity condition. Mean rates for visual-only (black), laser-only (green), and pair (blue for facilitation, red for suppression) are presented. Gray-shaded region denotes the 100–200 ms time window following onset of visual and optogenetic stimulation from which spike rates were calculated in (D).

(C and D) Best-fit visual (w_V) and optogenetic (w_L) weights according to each visual contrast and stimulation intensity condition across all 10,000 model-simulated neurons (C) and 43 recorded single units (D).

were qualitatively similar to the pattern obtained from the fits to the simulation and accounted for the majority of the variability in the data (mean explained variance = 89% ± 1.9% SE) (Figure 5D). Weights were consistently below unity, indicating a sub-additive interaction, and they depended systematically on contrast and stimulation intensity, with weights increasing with stimulus intensity for both laser and luminance contrast. Inspection of the average population responses for facilitated units indicated that near-equal weights for both visual and optogenetic responses resulted from intermediate contrasts and stimulation intensities that produced, on average, similar response magnitudes separately and as a pair (Figure 5A). For suppressed units, near-equal weights also resulted from intermediate contrasts and stimulation intensities, but for these units produced a pair response with magnitude roughly half-way between the two individual responses separately (Figure 5B). For both populations, the combined responses tended to approach the average of the two individual responses. For conditions of high visual contrast and low stimulation intensity or vice versa, weights diverged and took on values biased in favor of the higher of the

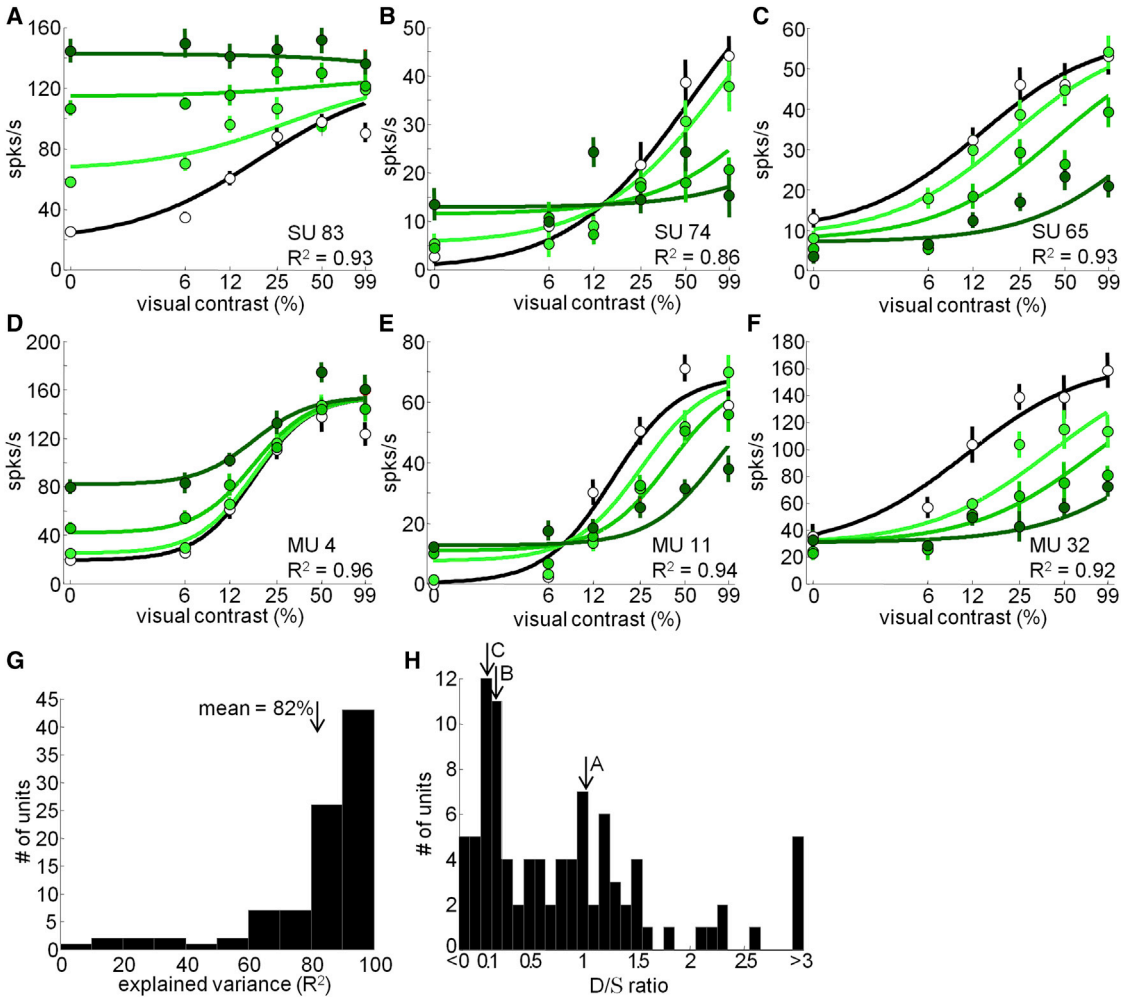

Figure 6. Normalization Model Accounts for Optogenetic Modulation of Visual Contrast Response Functions

(A–C) Single-unit example visual contrast response functions without optogenetic stimulation (black) and at three different stimulation intensity levels (different shades of green from light to dark indicate increasing intensity). Dots indicate mean rates ± SE. Curves produced from normalization model fits with explained variance (R^2) indicated.

(D–F) Same except for multi-unit recording sites.

(G) Distribution of explained variance (R^2) across the population (mean = 82% ± 2.1% SE). See also Figures S5 and S6.

(H) Distribution of D/S ratios obtained from normalization model fits across the population. Single-unit examples from (A)–(C) are indicated with downward arrows.

two. In these instances, the combined responses tended to behave according to a winner-take-all of the two individual responses separately. The observed range of competitive interactions between visual and optogenetic stimulation, from near-equal weighting to winner-take-all, was similar to the interactions described previously for multiple, overlapping, or adjacent visual stimuli (Reynolds and Desimone, 2003; Busse et al., 2009), suggesting that modulation of excitatory drive and divisive suppression, regardless of the source, is sufficient to generate similar phenomena.

The above analyses show that the model qualitatively captures visual-optogenetic interactions at the level of the population as a whole. To test the model's ability to fit individual neuron response patterns, we fit the normalization model to each unit in our entire dataset, across all visual contrasts and optogenetic stimulation intensities. All four contrast response functions were fit simultaneously (visual-only, low, mid, and high stimulation intensities) in order to find a single set of parameters that best fit the data for each unit. This allowed us to quantify how well the normalization model accounted for the observed response interactions across visual contrasts (c) and normalized stimulation intensity (λ). The model accounted for much of the variance in mean responses measured across visual contrast and stimulation intensity (mean explained variance = 82% ± 2.1% SE) (Figures 6A–6G). It significantly outperformed a simpler additive model in which optogenetic stimulation is represented as a constant additive or subtractive term dependent on stimulation intensity (Wilcoxon signed-rank test, $p = 0.007$) (Figure S5). One could imagine that as stimulation intensity increases, the enlargement of the illuminated region might result in additional

recruitment of excitatory and inhibitory neurons, causing variation in the ratio of stimulation-induced excitatory drive and divisive suppression. To allow for this, we tested a modified model in which the strength of drive and suppression (parameters D and S) were allowed to vary independently across different stimulation intensities. This alternative model did not improve the fits to the data enough to justify the additional degrees of freedom (Figure S6).

While we observed a range of effects of optogenetic stimulation on the visual contrast response functions, three distinct types of effects within this continuum are represented by the single-unit (Figures 6A–6C) and multi-unit (Figures 6D–6F) examples presented. For units that were facilitated at low (or zero) visual contrast by optogenetic stimulation, the magnitude of that facilitation tended to either reduce (Figures 6A and 6D) or turn into suppression (Figures 6B and 6E) at higher contrasts. Increasing stimulation intensity led to greater facilitation at low contrast and greater suppression at high contrast. For units that were suppressed or unaffected at low (or zero) visual contrast, increased suppression was observed at higher visual contrasts (Figures 6C and 6F). Again, the suppression observed at high contrast increased with increasing stimulation intensity. Both cases resulting in suppression at high visual contrast are reminiscent of previously reported response properties associated with cross-orientation suppression and surround suppression in V1 (Carandini et al., 1997; Cavanaugh et al., 2002). As expected, units that were facilitated across all visual contrasts were best fit by a laser-induced ratio of drive to suppression favoring excitatory drive (Figure 6H). For units that were facilitated at low contrast and suppressed at high contrast, the ratio favored suppression. Lastly, units that were suppressed across all visual contrasts were best fit by suppression with little or no excitatory drive. Together, these results suggest that optogenetic depolarization of excitatory neurons in V1 tapped into normalization circuitry and that modulation of excitatory drive and divisive suppression, regardless of the source, is sufficient to generate a variety of non-linear visual response properties associated with overlapping or adjacent visual stimuli.

Optogenetic Hyperpolarization and Normalization

To further test the normalization model, we performed similar experiments using the hyperpolarizing opsin eArch3.0 (Mattis et al., 2012) targeted to excitatory neurons in V1. We injected an adeno-associated virus (AAV5-CaMKIIα-eArch3.0-ts-EYFP) encoding eArch3.0 under control of the CaMKIIα promoter at a second, distant site within V1 in monkey A (Figure 1A). The virus injection and subsequent experimental protocols were identical to those described for the optogenetic depolarization experiments using C1V1 (see Supplemental Experimental Procedures). We recorded from 91 units (40 single neurons, 51 multi-units) within the stimulated patch of cortex and found that 22 units (18 single, 4 multi) were significantly modulated, relative to baseline, in response to the highest stimulation intensity tested (Wilcoxon rank-sum test, $p < 0.05$) (Figure 7B). The most common effect was a significant reduction in firing rate in response to light (20 units; 17 single, 3 multi), as might be expected following the activation of the hyperpolarizing opsin eArch3.0 (Figures 7A and 7B). The remaining 2 out of 22 units showed a significant increase in firing rate in response to light (2 units; 1 single, 1 multi), which presumably resulted from disinhibition due to reduced excitatory drive to inhibitory neurons. We did not commonly observe post-stimulation (10–210 ms following stimulation offset) effects on baseline activity as we did at the C1V1 recording site. Only 5 units (4 single, 1 multi) were significantly modulated during this post-stimulation period (Wilcoxon rank-sum test, $p < 0.05$), all of which were facilitated and never suppressed (Figure 7C).

We next examined the effect of optogenetic hyperpolarization of excitatory neurons on the visually evoked response. We measured visual-optogenetic interactions for a small dataset of 11 units, 9 of which were sensitive to both visual contrast and stimulation intensity and were therefore analyzed further (two-way ANOVA, $p < 0.05$). Two of these 9 units (1 single, 1 multi) were significantly modulated, relative to baseline, in response to the highest stimulation intensity tested (Wilcoxon rank-sum test, $p < 0.05$). Both of these units exhibited baseline suppression, as well as suppression of the visually evoked response for at least one luminance contrast (Wilcoxon rank-sum test, $p < 0.05$, Bonferroni corrected for multiple comparisons across visual contrasts) (example unit in Figure 7D). An additional 5 of the 9 units exhibited no stimulation effect at baseline (likely due to a floor effect caused by low baseline rates) but suppression during the visual response (example unit in Figure 7E). In no case did we observe facilitation of the visual response. The normalization model accounted for much of the variance in mean responses measured across visual contrast and stimulation intensity (mean explained variance = 86% ± 3.9% SE) (Figures 7D–7F), with similar performance to that obtained at the C1V1 recording site. In the case of the eArch3.0 recording site, the normalization and additive models provided comparably good fits (Wilcoxon signed-rank test, $p = 0.1$), with a single exception (Figures S5D and S5E). The contrast response functions of this neuron, with normalization and additive fits, appear in Figure 7E.

Changes in Drive and Suppression with Optogenetic Stimulation

We next analyzed how the drive (D) and suppression (S) parameters of the normalization model changed with optogenetic modulation of visual responses. In almost all units studied at the site of the depolarizing opsin (C1V1), effects of optogenetic stimulation on the visual contrast response functions were best fit by positive values of D, corresponding to an optogenetically induced increase in drive (83/93 units, 89%; mean value of D = 12.4 ± 2.8 SE) and positive values of S, corresponding to an increase in suppression (80/93 units, 87%; mean value of S = 14.1 ± 2.8 SE). At the eArch3.0 site, optogenetic activation caused more modest and less consistent changes in the D and S parameters, typically resulting in negative D parameter values (7/9 units, 78%; mean value of D = −0.09 ± 0.09 SE), consistent with the laser-induced reduction in excitatory drive expected following activation of the hyperpolarizing opsin eArch3.0. The S parameter values at the eArch3.0 recording site were negative in only a minority of cases (2/9 units, 22%; mean value of S = 1.1 ± 1.1 SE). Thus, while the majority of the neurons studied showed laser-induced changes that are consistent with

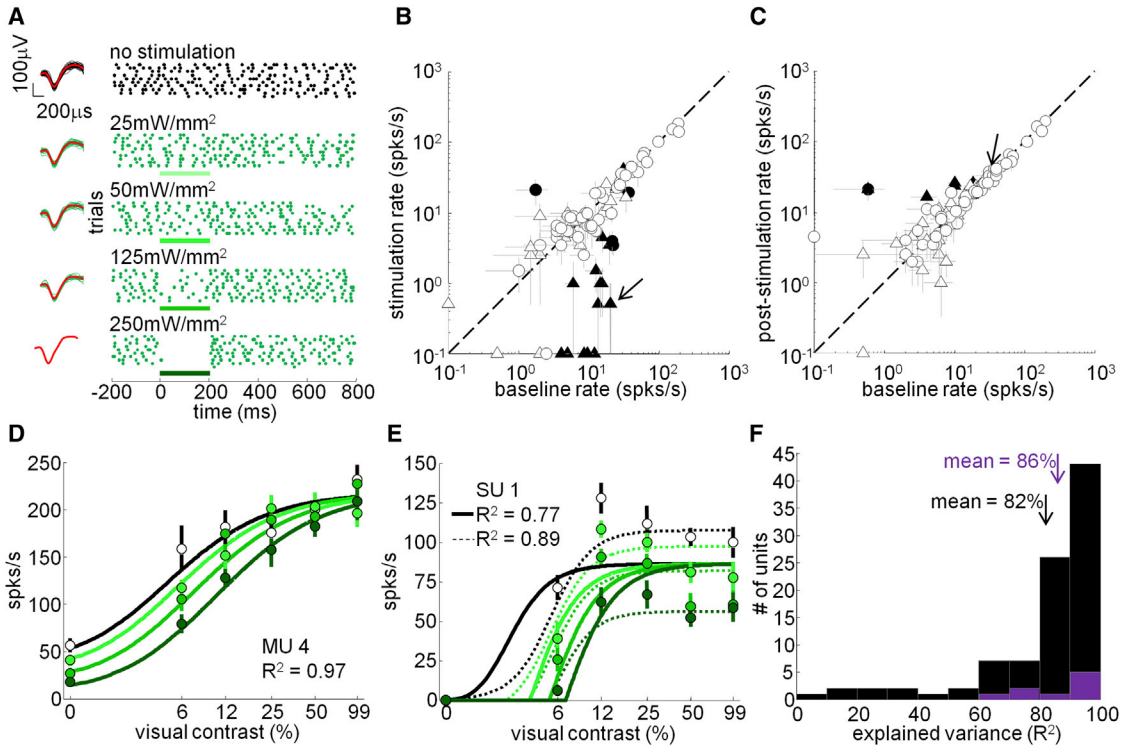

Figure 7. Normalization Model Accounts for Optogenetic Modulation of Visual Contrast Response Functions with the Hyperpolarizing Opsin eArch3.0

(A) Single-unit example from eArch3.0 site. Raster indicates the time of action potentials on trials with (green dots) or without (black) 200 ms continuous optogenetic stimulation. Each row is a separate trial. Four different stimulation intensities (25, 50, 125, and 250 mW/mm^2) were tested. The action potential waveforms associated with each stimulation condition are presented to the left of the rasters (average waveforms for each condition are in red).

(B) Mean ± SE rates with and without optogenetic stimulation (250 mW/mm^2) for the entire population (n = 91). Rates were calculated within a 200 ms time window aligned with stimulus onset. Arrow indicates single-unit example from (A). Triangles indicate single units, circles indicate multi-units, filled symbols indicate significant optogenetic modulation (Wilcoxon rank-sum test, $p < 0.05$).

(C) Same as in (B) but for a post-stimulation time window 10–210 ms following stimulation offset.

(D and E) Single-unit example visual contrast response functions without optogenetic stimulation (black) and at three different stimulation intensity levels (different shades of green from light to dark indicate increasing intensity). Dots indicate mean rates ± SE. Curves produced from normalization model fits with explained variance (R^2) indicated. Dashed curves in (E) produced from additive model fit.

(F) Distribution of explained variance (R^2) across the population for eArch3.0 experiments in purple (mean = 86% ± 3.9% SE) and for C1V1 experiments in black (mean = 82% ± 2.1% SE).

upregulation of drive (88/93 neurons) and suppression (80/93 units) by C1V1 activation, and downregulation of drive by eArch3.0 activation (7/9 units), the tendency for S to increase with eArch3.0 activation (7/9 units) underscores the potentially complex relationship between the highly abstract model parameters and the underlying circuit and biophysical mechanisms.

DISCUSSION

The present experiments provide direct evidence for a normalization computation originating from macaque V1. Optogenetic activation of excitatory drive in V1 induced several forms of response modulation that are consistent with the predictions of the normalization model, and parallel effects observed with elevations in luminance contrast. First, when presented on its own, without visual stimulus presentation, optogenetic depolarization of excitatory neurons could either facilitate or suppress baseline activity (Figure 2), suggesting that while the opsin was expressed almost exclusively in excitatory neurons, this activation of excitatory drive was accompanied by indirect activation of inhibition. These responses were intensity dependent, exhibiting a sigmoidal intensity response function, similar to the saturating contrast response function that is typically observed when varying the luminance contrast of a visual stimulus (Figure 3). Consistent with indirect activation of inhibition, simultaneous visual and optogenetic stimulation produced sub-additive pair responses that exhibited shifts in response weighting with changes in luminance contrast and stimulation intensity (Figures 4 and 5). The visual contrast response function was modulated in a number of different ways by optogenetic stimulation, including facilitation at low visual contrast and suppression at high visual contrast (Figure 6). Despite the heterogeneity of these effects, they can all be understood as natural properties of a normalization circuit. Accordingly, the above-described interactions between visual and optogenetic stimulation were predicted by a normalization model incorporating optogenetic stimulation as a source of

excitatory drive, which indirectly activated divisive suppression (Figures 4 and 5). This model was inspired by similar models that have been shown to account well for the interactions between multiple visual stimuli (Carandini et al., 1997). In fact, the current model essentially treated optogenetic stimulation as a second visual stimulus, substituting stimulation intensity for luminance contrast and assuming, for each neuron, a fixed ratio of laser-induced excitatory drive and divisive suppression, which varied across neurons. This relatively simple model was able to account for response interactions across a wide range of visual contrasts and optogenetic stimulation intensities, including both activation and inactivation of excitatory drive, for individual neurons as well as for the population as a whole (Figures 4, 5, 6, and 7).

Based on an earlier study in macaque frontal cortex (Han et al., 2009), we expected that lentivirus driving expression of opsin under the CaMKIIα promoter would lead to selective expression in excitatory neurons, and this was validated histologically (Figure 1B). Therefore, directly depolarized neurons were almost all excitatory and rarely, if ever, inhibitory. Light intensity falls off exponentially as it passes through cortical tissue (Yizhar et al., 2011a); therefore, only in superficial cortex would we have expected power density to remain above the minimum threshold necessary to activate C1V1 (Mattis et al., 2012). Thus, optogenetic stimulation most likely directly depolarized excitatory neurons in supragranular layers. Neurons within the input layer 4C and infragranular layer neurons lacking long apical dendrites were least likely to be directly depolarized due to the inability of light to effectively penetrate to the required cortical depth.

Optogenetic depolarization of excitatory neurons in V1 led to the indirect recruitment of both excitatory and inhibitory networks as evidenced by the suppression of spontaneous activity that we observed in a subset of the recorded population (Figure 2). Two previous studies reported similar suppression of spontaneous activity following optogenetic depolarization of excitatory neurons in macaque frontal cortex (Han et al., 2009; Ohayon et al., 2013). In both studies, expression of the depolarizing opsin channelrhodopsin-2 (ChR2) was targeted to excitatory neurons using the same CaMKIIα approach as used here. Thus, in those studies the observed suppression of spontaneous activity likely resulted from indirect activation of inhibitory neurons. Suppression of visually evoked activity has also been reported previously (Jazayeri et al., 2012), though in this case ChR2 was targeted to both excitatory and inhibitory neurons in macaque V1 using the human synapsin promoter. It is, therefore, difficult to know whether the suppression observed by Jazayeri and colleagues was due to direct depolarization of inhibitory neurons or via less direct pathways originating from depolarized excitatory neurons as in the current study. Contrary to these previous studies and the results presented here, suppression was not observed following optogenetic depolarization of excitatory neurons in superficial layers of tree shrew V1 (Huang et al., 2014). This may be due to the fact that stimulation was targeted to sites laterally offset from the recording site and it is known that cells in layer 2/3 of tree shrew V1 do not exhibit surround suppression (Chisum and Fitzpatrick, 2004). Several recent in vivo and in vitro studies in rodents have shown that optogenetic depolarization of layer 2/3 excitatory neurons leads primarily to inhibition rather than excitation in other layer 2/3 neurons (Mateo et al., 2011; Adesnik and Scanziani 2010; Beltramo et al., 2013). The indirect recruitment of inhibition is not at all surprising, as it has been known for some time now that feedforward and feedback inhibition are tightly coupled to the level of excitation in the local cortical network (Isaacson and Scanziani, 2011). Our results suggest that optogenetic depolarization of excitatory neurons in macaque V1 taps into this canonical motif of the cortical circuit.

Effects of optogenetic stimulation were likely, though not definitively, due to local circuit modulation within V1 rather than indirect activation of long-range cortico-cortical or cortico-thalamic circuits. We restricted our analysis of optogenetic modulation of visually evoked activity to a time window starting 100 ms after the onset of stimulation. This could, potentially, have allowed ample time for indirect activation of areas such as the LGN or V2, which provide strong feedforward and feedback inputs to V1, respectively. However, this is unlikely. First, it is unlikely that laser light penetrated deep enough into the cortex to directly activate cortico-thalamic neurons, either via their cell bodies situated in layer 6 or their apical dendrites, which terminate no higher than the top of layer 4 (Briggs, 2010). Second, cortico-thalamic feedback typically acts as a modulator, not a driver, of activity in the LGN (Guillery and Sherman, 2002). Modulators alter stimulus-evoked responses but do not change spontaneous activity. Cortico-thalamic feedback would not, therefore, be expected to alter baseline activity in the LGN and would not explain the facilitation and suppression of baseline activity that we often observed in V1 (Figure 2). While neurons projecting from V1 to V2 reside in superficial layers where they could have easily been directly activated by optogenetic stimulation, feedback from V2 to V1 is also modulatory and, again, would not be expected to alter baseline activity (Nassi et al., 2013). Finally, several control studies showed that effects of optogenetic stimulation on spontaneous and visually evoked activity were relatively fast in onset and stable in both magnitude and sign (Figures S2 and S4). If the observed effects had been due to the involvement of distant areas such as the LGN or V2, we might have expected effects to evolve more slowly and possibly even exhibit switches in sign across different time periods. However, this was not the case, suggesting that effects of optogenetic stimulation were primarily due to local circuit modulation within V1.

Simultaneous visual and optogenetic stimulation resulted in response interactions similar to those observed with multiple visual stimuli. In V1, these include cross-orientation suppression, whereby a non-preferred grating that generates either no response or a weak excitatory response on its own can become strongly suppressive when superimposed over a preferred grating (Morrone et al., 1982; Carandini et al., 1997). Similar results have been reported in V2, V4, MT, and inferior temporal cortex, for preferred and non-preferred stimuli placed adjacent to each other within a neuron's receptive field (Snowden et al., 1991; Miller et al., 1993; Rolls and Tovee, 1995; Reynolds et al., 1999; Heuer and Britten, 2002; Reynolds and Desimone, 2003). In all of these cases, the pair responses are almost always sub-additive and, in cases where contrast has been varied,

found to depend on the relative contrasts of the individual stimuli, according to a weighted sum (Reynolds and Desimone, 2003; Busse et al., 2009). The current study paralleled these earlier studies, but replaced one of the two visual stimuli with optogenetic depolarization of excitatory neurons, and found that optogenetic stimulation induced each of these types of response modulation (Figures 4 and 5). The sub-additivity we observed was not simply due to response saturation, as pair responses were found to be sub-additive across a wide range of stimulation intensities and visual contrasts, even those that produced individual responses well below maximum response (Figures 4E and 4F). For suppressed neurons, the pair response always fell somewhere between the responses to the individual stimuli presented on their own. Stimulation intensity or contrast could bias the pair response up or down in favor of the stimulus of higher salience (Figure 5B). This is similar to interactions reported previously for multiple visual stimuli (Reynolds and Desimone, 2003; Busse et al., 2009). However, for facilitated neurons, the pair response was typically higher than the responses to the individual stimuli on their own (Figure 5A). This is a departure from what has been reported previously for multiple visual stimuli and may be due to the strong excitatory contribution to the network from the sub-population of directly depolarized neurons. Given the relatively fast kinetics of the C1V1 opsin (Mattis et al., 2012), the excitatory effects of direct depolarization are expected to be absent post-stimulation, and only residual network effects are likely to remain. During this post-stimulation period immediately following optogenetic stimulation offset, pair responses for both the suppressed and facilitated populations typically fell between the responses to the individual stimuli on their own (Figure 5A). Thus, even for the facilitated population, once the excitatory effects of direct depolarization were removed, pair responses exhibited behavior similar to the pattern commonly observed with pairs of visual stimuli. Thus, similar response interactions were observed following the artificial form of activation produced by optogenetic stimulation. This provides strong evidence in favor of the normalization model's account for these phenomena: that they are governed by the ratio of excitatory drive and divisive suppression generated by each stimulus.

Though normalization has served as a helpful phenomenological description of visual stimulus interactions and other related phenomena, the underlying biophysical and circuit mechanisms involved remain poorly understood. We did find relatively systematic changes in normalization model parameters D and S that resulted from optogenetic modulation, with most neurons showing increases in drive and suppression upon optogenetic depolarization of excitatory neurons and reductions in drive upon optogenetic hyperpolarization of excitatory neurons. Though it might therefore be tempting to identify these parameters with the firing rates of excitatory and inhibitory neurons, caution is warranted here, especially in light of the modest increase in suppression (S) following eArch3.0-mediated hyperpolarization. The underlying circuitry that mediates normalization is potentially complex, and several different circuit motifs and biophysical mechanisms have been proposed as potentially contributing to the normalization computation in neocortical circuits (Carandini and Heeger, 2012). These include (1) shunting inhibition with increases in conductance resulting from either activation of channels with reversal potentials close to the resting potential or by concomitant increases in excitation and inhibition, (2) variation in conductance over time, or (3) synaptic depression. The extracellular recording data reported here are not well suited to distinguishing among these mechanisms.

Cross-orientation suppression, surround suppression, and the saturating nonlinearity of the contrast response function are all thought to rely on normalization computations (Carandini et al., 1997; Cavanaugh et al., 2002). In the case of cross-orientation suppression, contrast saturation and rectification in LGN relay cells can largely account for the response suppression measured in cat primary visual cortex (Priebe and Ferster, 2006). Nevertheless, there continues to be some debate regarding the degree to which cortex is involved, and few studies have addressed these questions in macaque (Priebe and Ferster, 2012; Smith et al., 2006). Our results suggest that local circuits within macaque V1 likely make an important contribution. Surround suppression has been the focus of several recent studies that have sought to elucidate the underlying circuits. Optogenetic studies in the mouse have implicated lateral excitatory inputs onto somatostatin-positive inhibitory neurons within V1 (Adesnik et al., 2012). Although optogenetic stimulation in the current study was centered over the recording site, the size of the illuminated patch of cortex was large enough to have potentially engaged a similar circuit. More recent work in the mouse has provided further support for the role of lateral connections in normalization (Sato et al., 2014). In this study, lateral connections within V1 were targeted via callosal projections originating from the opposite hemisphere. Interestingly, optogenetic stimulation of these lateral inputs modulated the visual contrast response functions of their neuronal targets in one of two ways, both of which were observed in the current study (Figures 6B, 6C, 6E, and 6F). A normalization model very similar to the one presented here was able to account for the effects observed by Sato and colleagues. This, again, suggests that optogenetic stimulation in the current study may have included activation of similar laterally projecting local circuit mechanisms (though see Huang et al., 2014). Recent studies in alert macaque have shown that cortico-cortical feedback contributes to surround suppression as well (Nassi et al., 2013). It has been proposed that feedback may set the spatial extent of normalization while lateral connections set the gain (Nassi et al., 2014). Future studies that can separately target lateral and feedback connections, as well as other neural elements, within the same experiment, will greatly advance our understanding of the complex circuit mechanisms underlying normalization in the primate cortex.

EXPERIMENTAL PROCEDURES

Surgical Procedures

Two adult male rhesus macaques (*Macaca mulatta*) were each implanted with a custom titanium head post and silicone-based artificial dura recording chamber over V1. We injected a VSVg-pseudotyped lentivirus carrying the C1V1-EYFP gene behind the 1.3 kb CaMKIIα promoter (lenti-CaMKIIα-C1V1$_{E162T}$-ts-EYFP; titer = 3 × 10^{10} TU/ml) into a single location in V1 in each of the two monkeys (monkeys A and M) while they were anesthetized and secured in a stereotactic frame. Injections of the same viral construct were made into V1 of one additional monkey in order to assess specificity of

viral expression to excitatory neurons. In a second, distant location in V1 of monkey A, we injected an adeno-associated virus carrying the eArch3.0-EYFP gene behind the 1.3 kb CamKIIα promoter (AAV5-CamKIIα-eArch3.0-ts-EYFP; titer = 4×10^{12} VP/ml).

Experimental and surgical procedures were approved by the Salk Institute Institutional Animal Care and Use Committee and conformed to NIH guidelines for the care and use of laboratory animals.

Histological Procedures

Sections were immunostained with primary antibodies against CaMKIIα, parvalbumin, calbindin, and calretinin. Confocal analysis was performed by taking 3D z stacks with a 63× oil lens.

Visual and Optogenetic Stimulation Protocol

Monkeys were alert and head restrained during all experiments. After isolating a single-unit or multi-unit cluster, we first assessed sensitivity to optogenetic stimulation. We randomly interleaved different stimulation intensities. Stimulation on each trial was continuous and lasted for 200 ms. Each condition was repeated at least five times.

For a subset of light-sensitive units, we proceeded to measure responses to simultaneous optogenetic stimulation and visual stimulus presentation. The presented visual stimuli consisted of circular patches of drifting sinusoidal gratings of mean luminance matching the surround (42 cd-m^2) at the optimal spatial and temporal frequencies. Each stimulus condition was presented at least five times. For simultaneous optogenetic stimulation and visual stimulus presentation, we varied the contrast of the presented gratings in log steps (0%, 6%, 12%, 25%, 50%, and 99%) and stimulated with four different intensities including zero. Visual contrast and stimulation intensity were randomly interleaved.

Data Analysis

Optogenetic stimulation response latency was calculated as described before (Lee et al., 2007; Sundberg et al., 2012). Only significantly facilitated single units were included in the latency histogram presented in the inset of Figure 2B. Significantly facilitated single and multi-units were included in the latency versus intensity plot in Figure 3A. The transient-to-sustained response ratio was calculated as the mean rate within the first 50 ms time window aligned with stimulation onset (transient response) divided by the mean rate within the last 50 ms time window aligned to end with stimulation offset (sustained response). This calculation was performed for significantly facilitated units only. The average Fano factor time courses presented in Figure 3C were calculated as the firing rate variance divided by the mean in non-overlapping 50 ms time bins, averaged across the population.

Intensity response functions were fit with a hyperbolic ratio function. Fits were performed for significantly facilitated units only. Goodness-of-fit was assessed by calculating the percentage explained variance as R^2 = [1 – (error sum of squares / total sum of squares)].

Normalization model simulations were performed by calculating responses according to the normalization model (Equation 1 in the main text) across the same six visual contrasts (normalized: 0, 0.06, 0.12, 0.25, 0.50, 0.99) and the four population median optogenetic stimulation intensities (normalized: 0, 0.13, 0.38, 1) used during C1V1 experiments. For each of 10,000 simulated neurons, we randomly assigned model parameter values from the following distributions: R_o: exponential distribution with mean equal to 10; R_m: normal distribution with mean equal to 60 and variance equal to 5; σ: exponential distribution with mean equal to 1; n and m: normal distribution with mean equal to 2 and variance equal to 0.5; and D and S: uniform distributions ranging from 0.1 to 10.

SUPPLEMENTAL INFORMATION

Supplemental Information includes Supplemental Experimental Procedures and six figures and can be found with this article online at http://dx.doi.org/10.1016/j.neuron.2015.05.040.

AUTHOR CONTRIBUTIONS

J.J.N. and J.H.R. designed research; J.J.N. performed research; J.J.N. and M.C.A. analyzed data; A.H.C. produced viral constructs; A.W.R. provided technical expertise related to artificial dura implant; and J.J.N. and J.H.R. wrote the paper.

ACKNOWLEDGMENTS

This research was supported by grants from the National Eye Institute (R01-EY021827, R21-EY020673, P30-EY-019005), R21 EY022853 (to A.W.R.), The Gatsby Charitable Foundation (to A.H.C. and J.H.R.), The Salk Institute Excellerators Fellowship Program (to J.J.N.), and the Swartz Foundation (to M.C.A.). Thanks to Dr. Karl Deisseroth for supplying the lentivirus plasmid, Drs. Thomas Albright, Gene Stoner, Octavio Ruiz, and Edward Callaway for their scientific expertise, Drs. Richard Born and Bryan Hansen for helpful comments on the manuscript, Lee Campbell and Bryan Nielsen for software/hardware development, the Salk Machine Shop for assistance in the design and manufacturing of custom parts, and Catherine Williams and the Salk Animal Resources Department for veterinary support.

Received: June 11, 2014
Revised: January 8, 2015
Accepted: May 21, 2015
Published: June 17, 2015

REFERENCES

Adesnik, H., and Scanziani, M. (2010). Lateral competition for cortical space by layer-specific horizontal circuits. Nature *464*, 1155–1160.

Adesnik, H., Bruns, W., Taniguchi, H., Huang, Z.J., and Scanziani, M. (2012). A neural circuit for spatial summation in visual cortex. Nature *490*, 226–231.

Albrecht, D.G., and Geisler, W.S. (1991). Motion selectivity and the contrast-response function of simple cells in the visual cortex. Vis. Neurosci. *7*, 531–546.

Beltramo, R., D'Urso, G., Dal Maschio, M., Farisello, P., Bovetti, S., Clovis, Y., Lassi, G., Tucci, V., De Pietri Tonelli, D., and Fellin, T. (2013). Layer-specific excitatory circuits differentially control recurrent network dynamics in the neocortex. Nat. Neurosci. *16*, 227–234.

Briggs, F. (2010). Organizing principles of cortical layer 6. Front. Neural Circuits *4*, 3, http://dx.doi.org/10.3389/neuro.04.003.2010.

Busse, L., Wade, A.R., and Carandini, M. (2009). Representation of concurrent stimuli by population activity in visual cortex. Neuron *64*, 931–942.

Carandini, M., and Heeger, D.J. (2012). Normalization as a canonical neural computation. Nat. Rev. Neurosci. *13*, 51–62.

Carandini, M., Heeger, D.J., and Movshon, J.A. (1997). Linearity and normalization in simple cells of the macaque primary visual cortex. J. Neurosci. *17*, 8621–8644.

Cavanaugh, J.R., Bair, W., and Movshon, J.A. (2002). Nature and interaction of signals from the receptive field center and surround in macaque V1 neurons. J. Neurophysiol. *88*, 2530–2546.

Chisum, H.J., and Fitzpatrick, D. (2004). The contribution of vertical and horizontal connections to the receptive field center and surround in V1. Neural Netw. *17*, 681–693.

Churchland, M.M., Yu, B.M., Cunningham, J.P., Sugrue, L.P., Cohen, M.R., Corrado, G.S., Newsome, W.T., Clark, A.M., Hosseini, P., Scott, B.B., et al. (2010). Stimulus onset quenches neural variability: a widespread cortical phenomenon. Nat. Neurosci. *13*, 369–378.

Douglas, R.J., and Martin, K.A. (2004). Neuronal circuits of the neocortex. Annu. Rev. Neurosci. *27*, 419–451.

Grossberg, S. (1973). Contour enhancement, short-term memory, and constancies in reverberating neural networks. Stud. Appl. Math. *52*, 217–257.

Guillery, R.W., and Sherman, S.M. (2002). Thalamic relay functions and their role in corticocortical communication: generalizations from the visual system. Neuron *33*, 163–175.

Han, X., Qian, X., Bernstein, J.G., Zhou, H.H., Franzesi, G.T., Stern, P., Bronson, R.T., Graybiel, A.M., Desimone, R., and Boyden, E.S. (2009). Millisecond-timescale optical control of neural dynamics in the nonhuman primate brain. Neuron *62*, 191–198.

Heeger, D.J. (1992). Normalization of cell responses in cat striate cortex. Vis. Neurosci. *9*, 181–197.

Heuer, H.W., and Britten, K.H. (2002). Contrast dependence of response normalization in area MT of the rhesus macaque. J. Neurophysiol. *88*, 3398–3408.

Huang, X., Elyada, Y.M., Bosking, W.H., Walker, T., and Fitzpatrick, D. (2014). Optogenetic assessment of horizontal interactions in primary visual cortex. J. Neurosci. *34*, 4976–4990.

Isaacson, J.S., and Scanziani, M. (2011). How inhibition shapes cortical activity. Neuron *72*, 231–243.

Jazayeri, M., Lindbloom-Brown, Z., and Horwitz, G.D. (2012). Saccadic eye movements evoked by optogenetic activation of primate V1. Nat. Neurosci. *15*, 1368–1370.

Lee, J., and Maunsell, J.H. (2009). A normalization model of attentional modulation of single unit responses. PLoS ONE *4*, e4651, http://dx.doi.org/10.1371/journal.pone.0004651.

Lee, J., Williford, T., and Maunsell, J.H. (2007). Spatial attention and the latency of neuronal responses in macaque area V4. J. Neurosci. *27*, 9632–9637.

Louie, K., Khaw, M.W., and Glimcher, P.W. (2013). Normalization is a general neural mechanism for context-dependent decision making. Proc. Natl. Acad. Sci. USA *110*, 6139–6144.

Mateo, C., Avermann, M., Gentet, L.J., Zhang, F., Deisseroth, K., and Petersen, C.C. (2011). In vivo optogenetic stimulation of neocortical excitatory neurons drives brain-state-dependent inhibition. Curr. Biol. *21*, 1593–1602.

Mattis, J., Tye, K.M., Ferenczi, E.A., Ramakrishnan, C., O'Shea, D.J., Prakash, R., Gunaydin, L.A., Hyun, M., Fenno, L.E., Gradinaru, V., et al. (2012). Principles for applying optogenetic tools derived from direct comparative analysis of microbial opsins. Nat. Methods *9*, 159–172.

Meskenaite, V. (1997). Calretinin-immunoreactive local circuit neurons in area 17 of the cynomolgus monkey, Macaca fascicularis. J. Comp. Neurol. *379*, 113–132.

Miller, E.K., Gochin, P.M., and Gross, C.G. (1993). Suppression of visual responses of neurons in inferior temporal cortex of the awake macaque by addition of a second stimulus. Brain Res. *616*, 25–29.

Morrone, M.C., Burr, D.C., and Maffei, L. (1982). Functional implications of cross-orientation inhibition of cortical visual cells. I. Neurophysiological evidence. Proc. R. Soc. Lond. B Biol. Sci. *216*, 335–354.

Nassi, J.J., Lomber, S.G., and Born, R.T. (2013). Corticocortical feedback contributes to surround suppression in V1 of the alert primate. J. Neurosci. *33*, 8504–8517.

Nassi, J.J., Gómez-Laberge, C., Kreiman, G., and Born, R.T. (2014). Corticocortical feedback increases the spatial extent of normalization. Front. Syst. Neurosci. *8*, 105, http://dx.doi.org/10.3389/fnsys.2014.00105.

Ohayon, S., Grimaldi, P., Schweers, N., and Tsao, D.Y. (2013). Saccade modulation by optical and electrical stimulation in the macaque frontal eye field. J. Neurosci. *33*, 16684–16697.

Priebe, N.J., and Ferster, D. (2006). Mechanisms underlying cross-orientation suppression in cat visual cortex. Nat. Neurosci. *9*, 552–561.

Priebe, N.J., and Ferster, D. (2012). Mechanisms of neuronal computation in mammalian visual cortex. Neuron *75*, 194–208.

Reynolds, J.H., and Desimone, R. (2003). Interacting roles of attention and visual salience in V4. Neuron *37*, 853–863.

Reynolds, J.H., and Heeger, D.J. (2009). The normalization model of attention. Neuron *61*, 168–185.

Reynolds, J.H., Chelazzi, L., and Desimone, R. (1999). Competitive mechanisms subserve attention in macaque areas V2 and V4. J. Neurosci. *19*, 1736–1753.

Rolls, E.T., and Tovee, M.J. (1995). The responses of single neurons in the temporal visual cortical areas of the macaque when more than one stimulus is present in the receptive field. Exp. Brain Res. *103*, 409–420.

Ruiz, O., Lustig, B.R., Nassi, J.J., Cetin, A., Reynolds, J.H., Albright, T.D., Callaway, E.M., Stoner, G.R., and Roe, A.W. (2013). Optogenetics through windows on the brain in the nonhuman primate. J. Neurophysiol. *110*, 1455–1467.

Sato, T.K., Häusser, M., and Carandini, M. (2014). Distal connectivity causes summation and division across mouse visual cortex. Nat. Neurosci. *17*, 30–32.

Smith, M.A., Bair, W., and Movshon, J.A. (2006). Dynamics of suppression in macaque primary visual cortex. J. Neurosci. *26*, 4826–4834.

Snowden, R.J., Treue, S., Erickson, R.G., and Andersen, R.A. (1991). The response of area MT and V1 neurons to transparent motion. J. Neurosci. *11*, 2768–2785.

Sperling, G., and Sondhi, M.M. (1968). Model for visual luminance discrimination and flicker detection. J. Opt. Soc. Am. *58*, 1133–1145.

Sundberg, K.A., Mitchell, J.F., Gawne, T.J., and Reynolds, J.H. (2012). Attention influences single unit and local field potential response latencies in visual cortical area V4. J. Neurosci. *32*, 16040–16050.

Van Brederode, J.F., Mulligan, K.A., and Hendrickson, A.E. (1990). Calcium-binding proteins as markers for subpopulations of GABAergic neurons in monkey striate cortex. J. Comp. Neurol. *298*, 1–22.

Van Essen, D.C., Newsome, W.T., and Maunsell, J.H. (1984). The visual field representation in striate cortex of the macaque monkey: asymmetries, anisotropies, and individual variability. Vision Res. *24*, 429–448.

Yizhar, O., Fenno, L.E., Davidson, T.J., Mogri, M., and Deisseroth, K. (2011a). Optogenetics in neural systems. Neuron *71*, 9–34.

Yizhar, O., Fenno, L.E., Prigge, M., Schneider, F., Davidson, T.J., O'Shea, D.J., Sohal, V.S., Goshen, I., Finkelstein, J., Paz, J.T., et al. (2011b). Neocortical excitation/inhibition balance in information processing and social dysfunction. Nature *477*, 171–178.

Zeki, S., and Shipp, S. (1988). The functional logic of cortical connections. Nature *335*, 311–317.

Zoccolan, D., Cox, D.D., and DiCarlo, J.J. (2005). Multiple object response normalization in monkey inferotemporal cortex. J. Neurosci. *25*, 8150–8164.